THE ASTROPHYSICAL JOURNAL, 347:L31–L34, 1989 December 1

MOLECULAR HYDROGEN AND OPTICAL IMAGES OF HH 7–11

PATRICK HARTIGAN,[1] SALVADOR CURIEL, AND JOHN RAYMOND[1]
Received 1989 July 6; accepted 1989 September 5

ABSTRACT

We compare flux-calibrated H_2 images of HH 7–11 with Hα and [S II] images taken nearly simultaneously. The brightest objects in H_2 also radiate optically. A bow shock with a magnetic precursor explains most of the existing observations of HH 7.

Subject headings: nebulae: individual (HH 7–11) — shock waves — stars: formation

I. INTRODUCTION

Young stars often drive bipolar outflows that become visible optically as jets and HH objects when shocks in the flow cool radiatively (e.g., Mundt 1988). Probably the most enigmatic HH objects are the so-called low-excitation objects, the prototypes of this class being HH 7–11 (Böhm, Brugel, and Mannery 1980). HH 7–11 have radial velocities and line profiles indicative of shock velocities ~ 100 km s^{-1} (Solf and Böhm 1987), but the spectra show strong [O I] and [S II] lines characteristic of a low-velocity (~ 30 km s^{-1}) shock. In principle, molecules can radiate much of the kinetic energy lost by gas entering the shock and help to produce a low-excitation spectrum. If this process is important in low-excitation HH objects, then one would expect H_2 emission to arise from the same region that produces the optical lines in low-excitation HH objects. Alternatively, H_2 line emission could form in oblique shocks that are entirely distinct from those exciting the optical lines (for example, if gas is entrained along the edges of an evacuated cavity), or be completely absent if none of the preshock gas is molecular and no molecules are formed on grains in the postshock flow.

It has been difficult to compare H_2 observations with optical data because of the large ($\sim 8''$) apertures typically used in the H_2 work, but the recent development of near-infrared array detectors makes detailed comparisons of optical and molecular line images possible. In this *Letter* we present nearly simultaneous images of HH 7–11 taken in the light of Hα, [S II], and H_2 $S(1)$. Except for HH 11, the Hα and [S II] images are similar to the H_2 image, suggesting that the shocks which produce the optical radiation also affect the H_2 emission. In what follows we present the images, describe the flux calibration procedure, and discuss possible interpretations for the existing data.

II. OBSERVATIONS AND DATA REDUCTION

The H_2, Hα, and [S II] images of HH 7–11 appear in Figures 1 (Plate L4) and 2. The optical images were obtained using the TI 2 CCD on the Kitt Peak 2.1 m telescope on 1988 December 28–29. We used a narrow Hα filter that excluded the neighboring [N II] lines; the [S II] filter was wide enough to include both the 6716 Å and the 6731 Å lines.

The infrared images [$S(1)$ and K] were taken 1988 November 27–28 with the 58 × 62 SBRC array on the 2.1 m telescope on Kitt Peak. A total of 18 5 minute exposures and one 10 minute exposure comprise the final co-added images in Figures 1 and 2. The IR images were flattened by subtracting a median-filtered image of blank sky frames taken with the same exposure time as the object frame. Photometry of the bright ($K = 7$) stars used for flux calibration (see below) appears to be reproducible to 2% or so between images. The seeing was 1″ for the optical images and 2″ for the IR images.

The IR field of view is roughly 45″ square. This is too small to include the entire HH 7–11 field, and care must be taken to combine the images correctly. In all but the extreme northwest image in the composite (where a telescope offset was needed to position the image) at least one of HH 7, SSV 13, or star 25 (see Fig. 1) is visible, allowing individual images to be embedded into a composite. The most uncertain alignment was the combination of the images near HH 7 with those near SSV 13 (where HH 10 was used for alignment). The stellar images in the composite have seeing profiles indistinguishable from those in the original images. The HH 7 area has roughly 45 minutes total exposure, HH 11 has 40 minutes, and the region to the northwest of SSV 13 has 15 minutes in all.

It is important to magnify the H_2 image to put it on the same scale in arcseconds per pixel as the optical images, and to check the rotation between the sets of images. Rotation and scale measurements cannot be done accurately using the HH 7–11 images owing to the paucity of stars appearing in both the optical and H_2 images. Instead, we measured the scale and rotation of the H_2 and optical images of Cepheus A, which has several stars that can be used for this purpose. The H_2 and optical images coincide when the H_2 images are rotated by 1°.9 and magnified by 1.87. We estimate that the final images in Figures 1 and 2 are aligned to $\pm 1''.0$.

We used photometry of Feige 110 (chosen for its featureless continuum at optical wavelengths) to calibrate the fluxes of the HH objects. The K magnitude of Feige 110 was 12.67 [3.39×10^{-16} ergs cm^{-2} s^{-1} Å^{-1} at $S(1)$, assuming equal $S(1)$ and K magnitudes; Rydgren *et al.* 1984]. We calibrated $S(1)$ line fluxes by knowing the filter bandpass and measuring the $S(1)$ counts for Feige 110. The above procedure assumes that the HH objects have no continuum and no lines except $S(1)$ passed by the filter. Since the filter transmission peaks at 2.122 μm with a FWHM of 0.027 μm, other emission lines do not contribute significantly to the observed counts. A large $K/S(1)$ ratio identifies the presence of a continuum component to the flux. Burton *et al.* (1989) found HH 7 to be a pure emission-line source, and the $K/S(1)$ photometry presented in Table 1 suggests that the other HH objects are similar in nature.

We observe 2.0×10^{-13} ergs cm^{-2} s^{-1} at $S(1)$ centering a 5″

[1] Visiting Astronomer, Kitt Peak National Observatory, operated by the National Optical Astronomy Observatory under contract to the National Science Foundation.

PLATE L4

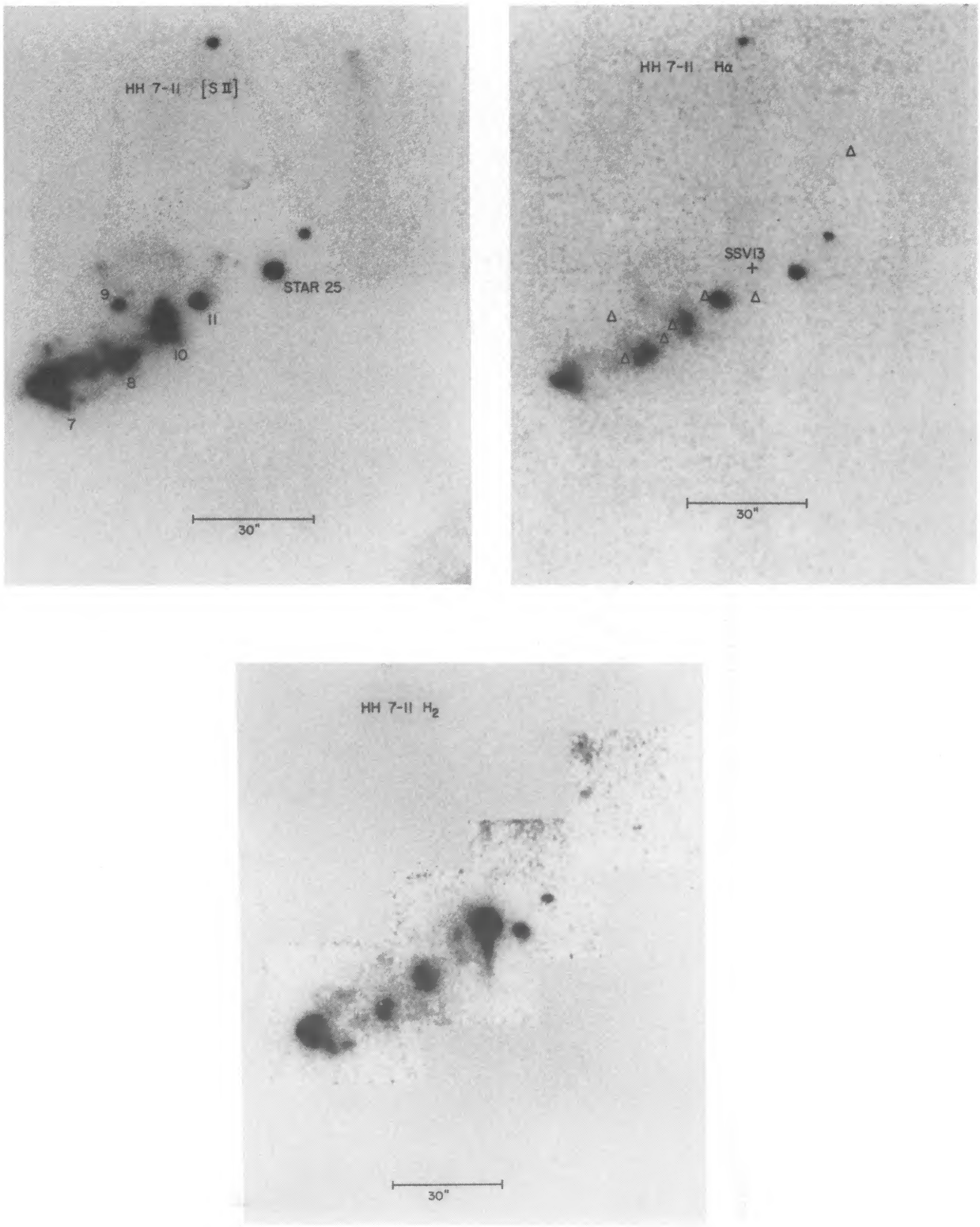

FIG. 1.—H_2 $S(1)$, [S II], and Hα images of the HH 7–11 region. HH 7, 8, and 10 are clearly visible in all three images. Positions of HCO^+ emission (Rudolph and Welch 1988) are marked with triangles; SSV 13, the bright infrared source in the H_2 image, is marked with a cross in the Hα image.

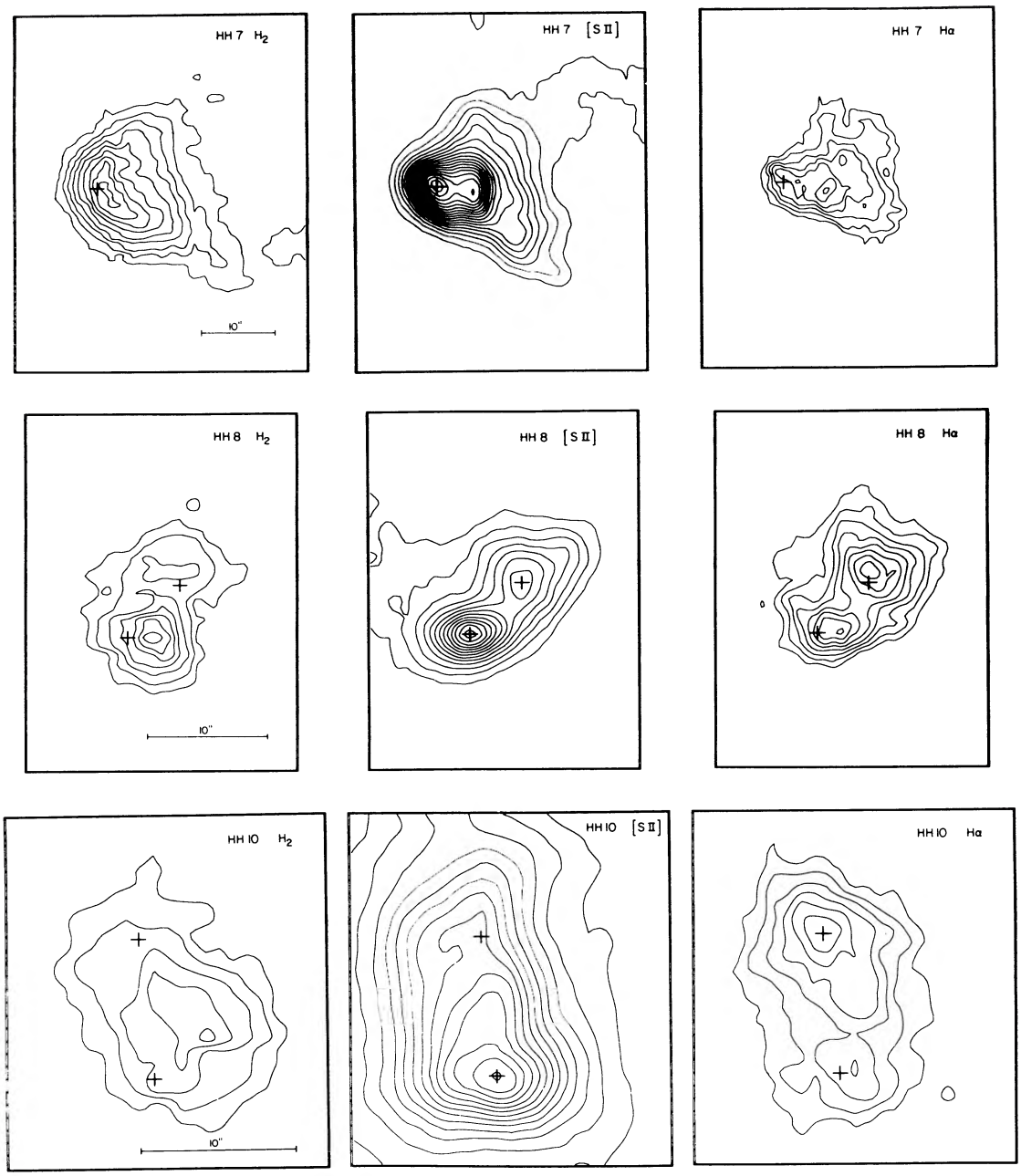

FIG. 2.—Contour plots of HH 7, 8, and 10 (cf. Fig. 1). The contours are linear and range from the surrounding sky level to the maximum intensity in each image. Fiducial marks denote prominent emission peaks in one of the filters. Plots for a given HH object have the same spatial scale.

TABLE 1

PHOTOMETRY

Object	K/H_2[a]	$S(1)$ Flux (10^{-13} ergs cm^{-2} s^{-1})
Gl 406	12.1	...
Feige 110	15.3	...
HD 1160	12.3	...
HH 7 (12″ aperture)	1.9	6.7
HH 7 (5″ aperture)	...	2.0
HH 8 (8″ aperture)	2.0	1.7
HH 10 (12″ aperture)	2.2	2.5

[a] Ratio of counts in the K and H_2 $S(1)$ images. The ratio is about 13 for most continuum sources, and roughly 2 for pure emission-line objects.

aperture on HH 7, in excellent agreement with Burton *et al.* (1989), who found an $S(1)$ flux for HH 7 of 1.8×10^{-13} ergs cm^{-2} s^{-1} within a 5″ aperture. Zealey, Williams, and Sandell (1984) observed 2.4×10^{-13} ergs cm^{-2} s^{-1} using a 12″ beam centered just south of HH 7. Without correcting for a continuum component (which should be negligible for HH 7–11) they find 9.6×10^{-13} ergs cm^{-2} s^{-1} from two overlapping beams that include HH 7. We measure 6.7×10^{-13} ergs cm^{-2} s^{-1} within a 12″ aperture centered on HH 7. Systematic errors, such as the assumption of the same magnitude for Feige 110 at K and $S(1)$, the flatness of the IR field, and uncertainties in the filter transmission curve dominate any statistical errors, which are a few percent or less for the HH objects. The fluxes in Table 1 should be good to 10%.

III. DISCUSSION

The optical and H_2 images of HH 7–11 appear in Figures 1 and 2. HH 7 is distinctly bow-shaped in all the images, with the H_2 and [S II] images coinciding to within an arcsecond. HH 7 has a bright secondary emission peak within the bow in the [S II] image. This peak is also bright in Hα, but disappears at H_2, making it a much higher excitation object than the remainder of HH 7. The higher excitation region of emission within the bow shock of HH 7 could come from jet gas cooling behind the jet's Mach disk. Hartigan (1989) has pointed out that the bow shock and Mach disk of a stellar jet should have comparable brightnesses for a wide range of initial conditions, and Raga (1988) has found Mach disk emission in his nonadiabatic jet models.

HH 8 consists of two distinct knots. The two knots have comparable brightnesses in Hα, but the southeastern knot is considerably brighter than the northwestern knot in [S II] and H_2. The knots are roughly coincident spatially except for HH 8SE, which is displaced 2″ to the east in [S II] (away from the exciting source) with respect to its Hα and H_2 photocenters. A clear gradient in excitation conditions also exists in HH 10, with the northern component bright in Hα and the southern portion bright in [S II]. The [S II] emission is located to the east of the H_2 emission in this object. HH 11 has only faint, extended H_2 emission, although it is the brightest of all the objects in Hα. This knot has a much higher radial velocity than the other HH objects and is more pointlike (cf. Solf and Böhm 1987).

Except for HH 11, regions with bright H_2 emission have optical counterparts. This suggests a common origin for the H_2 and optical lines. Draine, Roberge, and Dalgarno (1983) showed that a "magnetic precursor" can heat and compress gas in front of a shock wave moving through a weakly ionized gas with a transverse magnetic field. A jet moving through a magnetized molecular medium produces a substantial amount of H_2 emission from the precursor (even at high velocities close to the apex of the box shock). In this case, the H_2 lines are broader and have higher radial velocities than those expected in a bow shock model without a magnetic precursor, and the H_2 and optical emission should nearly coincide spatially (the H_2 emission is also bow-shaped).

We adopted a very simplified jet model with a magnetic precursor in which the temperature and density grow linearly through the precursor from T_0, n_0 to T_m, $n_m = 2n_0$, respectively, and then increase linearly through the shock until they reach their postshock values. Following Draine's (1980) analytical formulation, we find that a shock wave moving with a velocity 100 km s^{-1} in a molecular medium with a density 600 cm^{-3}, an ionization fraction 10^{-5}, a temperature $T_0 \sim 10$ K, and a magnetic field 70 μG produces a magnetic precursor with a maximum temperature 5000 K and a width 10^{16} cm.

We calculated the dissociation rates and population of the rotational-vibrational levels including collisions with electrons, and atomic and molecular hydrogen, throughout the precursor and shock front regions. The line ratios in Table 2 obtained with this simple model agree well with the 1–0 $S(1)$ line intensity in Table 1 and the 1–0 $S(1)$, 1–0 $S(0)$, 2–1 $S(1)$, and 1–0 $O(7)$ line intensities obtained by Burton *et al.* (1989). The optical spectrum of a shock with a magnetic precursor will have a lower excitation spectrum than a simple J-shock, since less energy is radiated in the optical lines when a precursor is present. The optical line widths observed in HH 7 indicate a shock velocity of 130–150 km s^{-1} although the optical spectrum resembles a 30 km s^{-1} shock (Solf and Böhm 1987). The infrared emission and dissociation energy of H_2 cannot account for this discrepancy, but excitation of the ultraviolet Lyman and Werner bands by electrons could carry away enough energy.

The above model predicts that the gas should already be moving at ~ 50 km s^{-1} with respect to the ambient cloud when it enters the J-shock that produces the optical lines. Hence, the velocity profiles for HH 7 should be *blueshifted* from the values predicted from bow shock models with a stationary medium. This removes the discrepancy Solf and Böhm (1987) observed between the radial velocities in HH 7, which are all blueshifted, and the predictions of a bow shock model, which include zero radial velocity for all orientation angles (Hartigan, Raymond, and Hartmann 1987; Raga and Böhm 1986). A magnetic precursor also predicts a line width for HH 7 of ~ 50 km s^{-1} in H_2, close to that observed by Zinnecker *et al.* (1989). A J-shock with a magnetic precursor seems to be a promising way to explain the [O I] 63 μm fluxes observed by Cohen *et al.* (1988) in HH 7.

Neither HH 8 nor HH 10 can be explained with a simple bow shock, since zero velocity is not included within the line profiles and the high radial velocity material does not occur closer to the star than the low radial velocity gas, as the bow shock models predict. Both objects have HCO^+ and H_2 $S(1)$ emission that concentrate to the south of the objects, with higher excitation material to the north. The simplest explanation seems to be to have a stellar wind from SSV 13 impact the side of a cavity, driving a shock into the high-density gas that gives rise to the HCO^+ and H_2 emission. The model is similar to a cloudet model like that proposed by Rudolph and Welch (1988), but the shock surrounding the "cloudlet" cannot be a simple bow shock. We see no easy way to understand the spatial separation of [S II] from the H_2 and Hα in these objects.

HH 11 is more enigmatic. This object cannot be a simple bow shock for the same reasons given for HH 8 and 10. We agree with Solf and Böhm (1987) that this object is most easily explained as a second ejection from SSV 13, but the only way we can think of to explain the observed 170 km s^{-1} line width and low-excitation spectrum without forming strong H_2 emission would be to have a *very* strong preshock magnetic field (~ 1 mG) for this object.

No bright H_2 emission is visible on the other side of SSV 13. Faint [S II] emission is visible 50″ northwest of SSV 13 near a faint wisp of H_2 (see Fig. 1). If an object as intrinsically bright as HH 7 were to exist within the area covered by our H_2 image it would have to be reddened by ~ 1.7 mag more than HH 7 at K, so $A_V \sim 20$.

IV. CONCLUSIONS

We have presented nearly simultaneous H_2 $S(1)$, [S II], and Hα images of the set of low-excitation HH objects HH 7–11.

TABLE 2

LINE FLUXES[a] FOR HH 7

Line	This *Letter*	Model	Burton *et al.*
1–0 $S(1)$	2.0(−13)	1.94(−13)	1.80(−13)
1–0 $S(0)$	...	5.78(−14)	4.38(−14)
2–1 $S(1)$	...	3.37(−14)	1.84(−14)
1–0 $O(7)$.....	...	2.06(−14)	1.94(−14)

[a] The fluxes are in ergs s^{-1} cm^{-2}.

Except for HH 11, regions with bright H_2 emission have optical counterparts, suggesting a common origin for the H_2 and optical lines. The existing data on HH 7 can be explained by a simple Mach disk/bow shock configuration at the end of a stellar jet; a magnetic precursor in front of the J-shock probably excites the H_2 lines observed in HH 7. This model explains the anomalous blueshifted radial velocities seen in HH 7 and provides a means to reconcile the low-excitation optical spectrum with the large line width observed.

The objects HH 8 and HH 10 show peculiar excitation gradients, with the lowest excitation spectrum occurring to the south in both objects where wind from the exciting star appears to shock against the walls of an evacuated cavity. The spatial and velocity characteristics of the emitting gas reveal a geometry more complex than a simple bow shock or planar shock. HH 11 remains an enigma, and could represent a second ejection from SSV 13. The low-excitation spectrum observed in this object is particularly difficult to explain since HH 11 has no visible H_2 emission.

It is a pleasure to acknowledge John Booth and Grace Wolf of the KPNO staff for their assistance with data acquisition, and Mike Merrill and Ron Probst for advice concerning data reduction. We are grateful to Ian Gatley and William Zealey for communicating their results prior to publication, and to Emilo Falco for his assistance in obtaining hard copies of the images presented in this *Letter*.

REFERENCES

Böhm, K.-H., Brugel, E. W., and Mannery, E. 1980, *Ap. J.* (*Letters*), **235**, L137.
Burton, M. G., Brand, P. W. J. L., Geballe, T. R., and Webster, A. S. 1989, *M.N.R.A.S.*, **236**, 409.
Cohen, M., Hollenbach, D. J., Haas, M. R., and Erickson, E. F. 1988, *Ap. J.*, **329**, 863.
Draine, B. T. 1980, *Ap. J.*, **241**, 1021.
Draine, B. T., Roberge, W. G., and Dalgarno, A. 1983, *Ap. J.*, **264**, 485.
Hartigan, P. 1989, *Ap. J.*, **339**, 987.
Hartigan, P., Raymond, J., and Hartmann, L. 1987, *Ap. J.*, **316**, 323.
Mundt, R. 1988, in *Formation and Evolution of Low Mass Stars*, ed. A. K. Dupree and M. T. V. T. Lago (Dordrecht: Kluwer), p. 257.
Raga, A. C. 1988, *Ap. J.*, **335**, 820.
Raga, A. C., and Böhm, K.-H. 1986, *Ap. J.*, **308**, 829.
Rudolph, A., and Welch, W. J. 1988, *Ap. J.* (*Letters*), **326**, L31.
Rydgren, A. E., Schmelz, J. T., Zak, D. S., and Vrba, F. J. 1984, *Pub. US Naval Obs.*, 2d Ser., Vol. **25**, No. 1.
Solf, J., and Böhm, K.-H. 1987, *A.J.*, **93**, 1172.
Zealey, W. J., Williams, P. M., and Sandell, G. 1984, *Astr. Ap.*, **140**, L31.
Zinnecker, H., Mundt, R., Geballe, T. R., and Zealey, W. J. 1989, *Ap. J.*, **342**, 337.

SALVADOR CURIEL, PATRICK HARTIGAN, and JOHN RAYMOND: Harvard-Smithsonian Center for Astrophysics, Mail Stop 16, 60 Garden Street, Cambridge MA 02138